Atmos. Chem. Phys. Discuss., doi:10.5194/acp-2016-520, 2016
Manuscript under review for journal Atmos. Chem. Phys.
Published: 22 June 2016

Atmospheric Chemistry and Physics Discussions

Lidar detection of high concentrations of ozone and aerosol transported from Northeast Asia over Saga, Japan

Osamu Uchino[1, 2], Tetsu Sakai[2], Toshiharu Izumi[2], Tomohiro Nagai[2], Isamu Morino[1], Akihiro Yamazaki[2], Makoto Deushi[3], Keiya Yumimoto[2], Takashi Maki[2], Taichu Y. Tanaka[2], Taiga Akaho[4], Hiroshi Okumura[4], Kohei Arai[4], Takahiro Nakatsuru[1], Tsuneo Matsunaga[1], Tatsuya Yokota[1]

[1]National Institute for Environmental Studies, 16-2 Onogawa, Tsukuba, Ibaraki 305-8506, Japan
[2]Meteorological Research Institute, 1-1 Nagamine, Tsukuba, Ibaraki 305-0052, Japan
[3]Japan Meteorological Agency, 1-3-4 Otemachi, Chiyoda-ku, Tokyo 100-8122, Japan
[4]Saga University, 1 Honjou, Saga, Saga 840-8502, Japan

Correspondence to: O. Uchino (uchino.osamu@nies.go.jp)

Abstract. To validate products of the Greenhouse gases Observing SATellite (GOSAT), we observed vertical profiles of aerosols, thin cirrus clouds, and tropospheric ozone with a mobile lidar system that consisted of a two-wavelength (532 and 1064 nm) polarization lidar and a tropospheric ozone Differential Absorption Lidar (DIAL). We used these lidars to make continuous measurements over Saga (33.24°N, 130.29°E) during 20–31 March 2015. High ozone and high aerosol concentrations were observed almost simultaneously in the altitude range 0.5–1.5 km from 03:00 to 20:00 Japan Standard Time on 22 March 2015. The maximum ozone volume mixing ratio was ~110 ppbv. The maxima of the aerosol extinction coefficient and optical depth at 532 nm were 1.2 km^{-1} and 2.1, respectively. Backward trajectory analysis indicated that an air mass with high ozone and aerosol concentrations could have been transported from Northeast Asia. Based on the lidar data and the ground-based in-situ measurements at Saga, this air mass could have been transported to the surface by vertical mixing when the planetary boundary layer developed in the daytime. This plume, which contained high ozone and aerosol pollutant concentrations, impacted surface air quality substantially. After some modifications of its physical and chemical parameters, the Meteorological Research Institute Chemistry-Climate Model, version 2 (MRI-CCM2) approximately reproduced the high-ozone volume-mixing ratio. The Model of Aerosol Species IN the Global AtmospheRe (MASINGAR) mk-2 successfully predicted high aerosol concentrations, but the predicted peak aerosol optical thickness was about one-third of the observed value.

Atmos. Chem. Phys. Discuss., doi:10.5194/acp-2016-520, 2016
Manuscript under review for journal Atmos. Chem. Phys.
Published: 22 June 2016

Atmospheric Chemistry and Physics Discussions

1 Introduction

Tropospheric ozone is a major air pollutant and impacts human health and vegetation (HTAP, 2010; Yue and Unger, 2014). It is also an important greenhouse gas (IPCC, 2013). Tropospheric aerosols are also air pollutants and aggravate respiratory conditions (HTAP, 2010). Tropospheric aerosols also enhance radiative forcing in a negative (sulfuric acid particles) or positive (black carbon) way (IPCC, 2013), and they affect remote sensing such as the measurement of greenhouse gases from space (Houweling et al., 2005; Uchino et al., 2012a). It is therefore very important to monitor tropospheric ozone and aerosols and to understand their temporal and spatial variations.

To validate products of the Greenhouse gases Observing SATellite (GOSAT), we developed a two-wavelength (532 and 1064 nm) polarization lidar (hereafter abbreviated as Mie lidar) to observe vertical profiles of tropospheric and stratospheric aerosols and thin cirrus clouds at the National Institute for Environmental Studies (NIES), Tsukuba (36.05°N, 140.13°E), Japan in 2009. In 2010 we also developed a DIfferential Absorption Lidar (DIAL) to measure tropospheric ozone profiles (hereafter abbreviated as ozone DIAL). The ozone DIAL was installed in a container with the Mie lidar. In March 2011, we moved the lidar container to Saga (33.24°N, 130.29°E) in the Kyushu district of western Japan at a location 2.6 m above sea level. The ozone DIAL was modified in September 2012 (Uchino et al., 2014).

Mie lidar has been used to demonstrate the influence of high-altitude aerosols and cirrus clouds on the GOSAT product of the column-averaged dry air mole fraction of carbon dioxide (XCO_2) retrieved from the Thermal And Near infrared Sensor for carbon Observation-Fourier Transform Spectrometer (TANSO-FTS) Short-Wavelength InfraRed (SWIR) spectral data onboard GOSAT. The XCO_2 data were improved by taking the vertical profiles of aerosols and cirrus clouds measured by Mie lidar into account (Uchino et al., 2012a). The increases of stratospheric aerosols caused by the 2009 Sarychev eruption and the 2011 Nabro eruption were observed by Mie lidar (Uchino et al., 2012b).

Ozone DIAL has been used to validate the GOSAT ozone product retrieved from TANSO-FTS Thermal InfraRed (TIR) spectral data (Ohyama et al., 2012), to observe ozone concentrations in the lower troposphere, and to compare the observed concentrations with those predicted by the Meteorological Research Institute Chemistry-Climate Model, version 2 (MRI-CCM2) (Deushi and Shibata, 2011). Use of Mie lidar and ozone DIAL will facilitate satellite product validation not only for GOSAT but also for upcoming satellites such as the TROPOspheric Monitoring Instrument (TROPOMI, Veefkind et al., 2012) and the Geostationary Environment Monitoring Spectroscopy (GEMS, Bak et al., 2013).

In this paper we report an event during which high concentrations of ozone and aerosols were observed almost simultaneously below an altitude of 1.5 km over Saga on 22 March 2015, which substantially impacted surface air quality. We also compared the observational results with those simulated by the models.

Atmos. Chem. Phys. Discuss., doi:10.5194/acp-2016-520, 2016
Manuscript under review for journal Atmos. Chem. Phys.
Published: 22 June 2016

Atmospheric Chemistry and Physics Discussions

2 Lidar system and observations

Mie lidar and ozone DIAL were installed in a container with dimensions of about 228 cm (width), 683 cm (length), and 255 cm (height), as shown in Fig. 1. Mie lidar is a two-wavelength (532 and 1064 nm) polarization lidar based on a neodymium-doped yttrium-aluminum-garnet (Nd:YAG) laser; the characteristics are summarized in Table 1. The output energy at 532 and 1064 nm was 130 mJ, with a pulse repetition rate of 10 Hz. The diameter of the receiving telescope was 30.5 cm. The output signals from the photomultiplier tubes (PMT) and a silicon avalanche photodiode (APD) were processed by transient recorders with a 12-bit analog/digital converter and a photon counter.

The ozone DIAL consisted of a Nd:YAG laser and a 2-m-long Raman cell filled with CO_2 gas that generated four Stokes lines from stimulated Raman scattering by CO_2 ; the characteristics are summarized in Table 2. In this study, we used three Stokes lines (276, 287, and 299 nm). The output energies of these Stokes lines were about 8–9 mJ per pulse, with a pulse repetition rate of 10 Hz. The receiving telescope diameters were 10 cm for boundary layer ozone measurements and 49 cm for free tropospheric ozone measurements. The output signals from the PMTs were also processed by transient recorders with a 12-bit analog/digital converter and a photon counter. The data analysis methods of Mie lidar and ozone DIAL have been described by Uchino et al. (2012b) and Uchino et al. (2014), respectively. The Mie lidar and ozone DIAL were synchronized by two pulse-delay generators. Next, we report the continuous lidar observational results made at Saga from 20 March to 31 March 2015.

3 Ozone DIAL data

Figure 2a shows a time-altitude cross-section of ozone volume mixing ratios observed by DIAL at Saga from 11:10 JST on 20 March to 14:33 JST on 31 March 2015. Lidar observations were not obtained from 15:56 JST on 27 March to 21:58 JST on 29 March 2015, mainly because of bad weather conditions. The vertical resolution was 270 m between altitudes of 450 m and 2 km and 540 m between altitudes of 2 and 6 km. The time resolution was set to 1 h to facilitate comparison with the MRI-CCM2. We made quality checks of the DIAL data. The gray regions in Fig. 2a correspond to areas where there were no observational data or the errors were larger than 10%. The errors were equated to 100% times the lidar signal-to-noise ratios. Regions surrounded by a black rectangle are areas where the data were affected by aerosols and/or clouds. In the lowest row of Fig. 2a, we show hourly data of surface oxidant volume mixing ratios (Ox) at Takagimachi in Saga city measured by the Saga Prefectural Environmental Research Center (https://www.pref.saga.lg.jp/web/at-contents/kankyo1/shisetsu/_40810/_41304/_67819.html). Takagimachi is located about 2.8 km northeast from the ozone DIAL site. Because the contribution of other components such as peroxyacetyle nitrate (PAN) to oxidant concentrations was

Atmos. Chem. Phys. Discuss., doi:10.5194/acp-2016-520, 2016
Manuscript under review for journal Atmos. Chem. Phys.
Published: 22 June 2016

extremely low, the oxidant volume mixing ratio was considered to be that of ozone.

Figure 2a indicates that the ozone volume mixing ratios measured by DIAL were usually about 50–70 ppbv during the study period. Comparatively high ozone concentrations, >75 ppbv, were detected at altitudes of 0.5–3 and 0.5–2 km on 20–23 March and 30–31 March, respectively. Notably high ozone volume mixing ratios of 90–110 ppbv at altitudes of 0.5–1.5 km were observed from 03:00 to 20:00 JST on 22 March. These high ozone concentrations were also seen in the surface photochemical oxidants data, i.e., the Ox equaled 92–101 ppbv from 15:00 to 21:00 JST on 22 March, as shown in the lowest row in Fig. 2a. The maximum concentration of Ox was 101 ppbv at 16:00 JST. This maximum value was far above the environmental quality standard of 60 ppbv for hourly photochemical oxidants in Japan (https://www.env.go.jp/en/air/aq/aq.html). These observational results show the descent of regions of high ozone concentrations and suggest that air with high ozone concentrations was transported to the surface by vertical mixing when the planetary boundary layer developed during the daytime.

3.1 Comparison of DIAL data with MRI CCM-2

The MRI-CCM2 is a global model that simulates chemical and physical processes that affect the distribution and evolution of ozone and other trace gases from the surface to the stratosphere (Deushi and Shibata, 2011). Uchino et al. (2014) have provided an outline of MRI-CCM2. The vertical resolution of the model increases from about 100 to 600 m from the surface to 6 km. The time step of the transport (chemistry) scheme is 30 (15) min. We used hourly model output data. The horizontal resolution is about 110 km. We examined whether or not the model could simulate DIAL observational results. The MRI-CCM2 simulated the DIAL observations reasonably well. However, the MRI-CCM2 could not reproduce the high ozone concentrations of 90–110 ppbv observed below an altitude of 1.5 km during 03:00–20:00 JST on 22 March 2015.

We therefore performed some simulations in which we changed the emission inventory data and the term that forced the reanalysis wind field. The most reasonable results were obtained when the following changes were made (Fig. 2b). The e-folding time of the nudging term was changed from 18 hours to 12 hours to more strongly force the simulated wind fields toward the reanalysis data. In addition, we changed the emission inventory of Regional Emission inventory in Asia version 1.1 (REAS 1.1) (Ohara et al., 2007) to REAS 2.1 (Kurokawa et al., 2013) and the NO_2/NO_x emissions ratio from 5% to 15% by volume, which is within the range of uncertainty (Carslaw, 2005). The emission inventory of NO_x increased about 50% from REAS 1.1 to REAS 2.1. Figure 2c shows the differences between the observed and simulated ozone mixing ratios. Simulated ozone volume mixing ratios were about 60–70 ppbv below an altitude of 1.5 km from 14:00 JST on 21 March to 21:00 JST on 22 March 2015, lower by about 20–50 ppbv compared with the DIAL results. A model with higher horizontal resolution might be necessary to more realistically simulate high surface ozone concentration events in the planetary boundary layer.

Atmos. Chem. Phys. Discuss., doi:10.5194/acp-2016-520, 2016
Manuscript under review for journal Atmos. Chem. Phys.
Published: 22 June 2016

Atmospheric Chemistry and Physics Discussions

4 Mie lidar data

First, we summarize the physical parameters obtained by Mie lidar. The backscattering ratio R is defined as

$$R = (BR + BA)/BR, \quad (1)$$

where BR and BA are the Rayleigh and Mie backscattering coefficients, respectively. Backscattering ratio profiles were derived by the inversion method (Fernald, 1984). We assumed the lidar ratio S (extinction-to-backscatter ratio) for aerosols to be 50 sr at 532 nm and 45 sr at 1064 nm (Sakai et al., 2003; Cattrall et al., 2005). To calculate BR, we used the atmospheric molecular density profiles obtained by operational radiosondes at the Fukuoka District Meteorological Observatory (33.58°N, 130.38°E). The aerosol extinction coefficient was calculated by multiplying BA by S.

The total volume depolarization ratio D was defined as

$$D = \mathrm{S} / (P + S) \cdot 100\ (\%), \quad (2)$$

where P and S are the parallel and perpendicular components of the backscattered signals, respectively. The particle depolarization ratio D_p was obtained from the equation

$$D_p = (D \cdot R - D_m)/(R - 1), \quad (3)$$

where D_m is the atmospheric molecular depolarization ratio. We used a D_m value of 0.37% for this lidar system; we calculated D_m from the spectral transmission data of the interference filter at 532 nm and the Rayleigh backscattering cross sections (Sakai et al., 2003). The value of D_p indicates whether the particles are spherical or non-spherical; large values indicate the presence of non-spherical particles. The wavelength exponent, Alp, shows whether small or large particles account for most of the Mie particles and is defined by

$$BA(\lambda) \propto \lambda^{-Alp}, \quad (4)$$

where λ is the wavelength. Larger values of Alp indicate the predominance of smaller (i.e., submicrometer-sized) particles.

Figures 3a and 3b show time-altitude cross-sections of the backscattering ratio (R) and the total volume depolarization ratio (D), respectively, observed by Mie lidar at Saga from 11:10 JST on 20 March to 14:33 JST on 31 March 2015. Mie lidar observation were not obtained from 15:56 JST on 27 March to 21:58 JST on 29 March 2015, mainly because of bad

Atmos. Chem. Phys. Discuss., doi:10.5194/acp-2016-520, 2016
Manuscript under review for journal Atmos. Chem. Phys.
Published: 22 June 2016

Atmospheric Chemistry and Physics Discussions

weather conditions. The vertical resolution was 150 m, and the time resolution was set to be 1 h for comparison with the Model of Aerosol Species in the Global Atmosphere (MASINGAR)-mk2 (Yukimoto et al., 2012). We made quality checks of Mie lidar data. Gray regions are areas where there were no observational data or the data were affected by clouds.

Aerosol layers with R in the range 2–4 almost always existed below an altitude of 2.5 km. An event of high aerosol loading with large values of R (~4–19) was observed below altitudes of 1.5 km on 22 March, when the values of D were small (1–6%) compared with those before and after the event, when the values of D were larger than ~8%. The main aerosol component during the event may have been submicrometer-sized spherical sulfate particles, because D_p was small (1–6%), and the wavelength exponent *Alp* was large (~1.4). In contrast, the main aerosol particles before and after the event were assumed to be supermicrometer-sized, nonspherical mineral dust particles because D_p was comparatively large (~13%) and *Alp* was approximately 1.0.

Hourly values of the mass concentrations of particulate matter with a diameter of 2.5 μm or less ($PM_{2.5}$) at Takagimachi measured by the Saga Prefectural Environmental Research Center were 23 μg m^{-3} at 10:00 JST and increased up to a maximum value of 110 μg m^{-3} at 15:00 JST on 22 March; the concentrations were greater than 82 μg m^{-3} during 13:00–16:00 JST and decreased to 17 μg m^{-3} at 01:00 JST on 23 March. The daily mean value of $PM_{2.5}$ was 50.6 μg m^{-3} for 24 hours on 22 March at Takagimachi, larger than the environmental quality standard of 35 μg m^{-3} in Japan (https://www.env.go.jp/en/air/aq/aq.html). Consideration of the lidar data and the temporal variation of $PM_{2.5}$ at Takagimachi suggests that air with high concentrations of both aerosols and ozone was transported to the surface by vertical mixing when the planetary boundary layer developed in the daytime.

4.1 Comparison of Mie lidar data with MASINGAR mk-2

The MASINGAR-mk2 is an improved version of the MASINGAR aerosol model (Tanaka et al., 2003); it treats five aerosol species: sulfate, black and organic carbon, sea salt, and soil dust. We used emission data for sulfur dioxide and for black and organic carbon from MACCity (Granier et al., 2011). Soil dust and sea salt were represented by 10 bins with particle diameters of 0.2–20 μm. The model was coupled online with the atmospheric general circulation model MRI-AGCM3 (Yukimoto et al., 2012). The horizontal resolution of the MASINGAR-mk2 was about 60 km, and the number of vertical layers was 40 from the surface to 0.1 hPa. The vertical resolutions were 100, 300, and 600 m at the lowest level and altitudes of 1 and 6 km, respectively. The time step of the transport (chemistry) scheme was 450 seconds, and we used hourly model output data.

Figures 4a and 4b show the time-height cross sections of aerosol extinction coefficients observed by Mie lidar and simulated by MASINGAR-mk2, respectively. Figure 4c represents the difference between the observed and simulated extinction coefficients. The model was able to capture the general characteristics of the observational results rather well. A close look at Fig. 4c reveals that the model underestimated the aerosol extinction coefficients of the anthropogenic pollutant

Atmos. Chem. Phys. Discuss., doi:10.5194/acp-2016-520, 2016
Manuscript under review for journal Atmos. Chem. Phys.
Published: 22 June 2016

event on 22 March but slightly overestimated the extinction coefficients associated with particles having larger total volume depolarization ratios on 30 and 31 March (i.e., dust-dominant case).

4.2 Comparison of aerosol optical depths

Figure 5 shows temporal variations of the aerosol optical depths (AOD) measured by Mie lidar at 532 nm and sky radiometer at 500 nm (Kobayashi et al., 2006, Uchino et al., 2012a) and simulated at 550 nm by MASINGAR-mk2 from 20 to 31 March. To estimate AODs from the lidar data, the extinction coefficient at 225 m was extrapolated to the ground, the extinction coefficient from 15 to 35 km was observed at night on the same day, and S was assumed to be 50 sr for all altitudes. When clouds and thick aerosols were present, AODs were not obtained. The sky radiometer was positioned on the roof of the building, which is four stories high and located to the west of the container (brown building in Fig. 1). Although it must be noted that the measured and simulated wavelengths differed slightly, the AODs were almost the same, except for the high aerosol and ozone event on 22 March. The maximum values of the AODs were 2.1 at 12:00 JST by lidar, 1.92 at 13:00 JST by sky radiometer, and 0.53 at 13:00 JST by MASINGAR-mk2. The model underestimated the AODs by factors of about 3.6–4 compared to the sky radiometer and lidar observations. One plausible explanation is that the model resolution (about 60 km) was insufficient to reproduce the observed prominent peak in which the observed AOD increased from 1.0 to 2.0 in 6 hours. In addition, inadequacies of the input anthropogenic emissions may partly explain the underestimate. To solve this problem, for example, it might be better to use the near real-time satellite data of sulfur dioxide and nitrogen dioxide provided by the Ozone Monitoring Instrument (OMI) onboard NASA's Aura satellite (Krotkov et al., 2016).

5 Discussion and concluding remarks

By using ozone DIAL and a two-wavelength polarization (Mie) lidar, we made continuous measurements of ozone and aerosol concentrations over Saga during 20–31 March 2015, with the exception of a period with bad weather conditions. High ozone and high aerosol concentrations that occurred nearly simultaneously were observed in the altitude range 0.5–1.5 km from 03:00 to 20:00 JST on 22 March 2015. The ozone volume mixing ratio was larger than 100 ppbv. The aerosol extinction coefficient and AOD at 532 nm were larger than 0.5 km^{-1} and 1.5, respectively.

To identify the origin of the ozone and aerosols and related transport processes, three-dimensional backward trajectories of air parcels were calculated with the NOAA Hybrid Single Particle Lagrangian Integrated Trajectory (HYSPRIT) model (Draxler and Hess, 1998; Stein et al., 2015), as shown in Fig. 6. Twenty-seven air parcels were initially left at altitudes of 600–1000 m over the lidar site at Saga. The trajectories were calculated for three days from 00:00 UTC (09:00 JST) on 22 March 2015. Based on the results of the backward trajectories, the high ozone and aerosol concentrations on 22 and 31

Atmos. Chem. Phys. Discuss., doi:10.5194/acp-2016-520, 2016
Manuscript under review for journal Atmos. Chem. Phys.
Published: 22 June 2016

March could have been transported from Northeast Asia. According to the ozonesonde measurements made by Wang et al. (2012), ozone concentrations ≥90 ppbv were observed over Beijing, China in late March. Ma et al. (2016) reported a significant increase of surface ozone from 2003 to 2015 at Shangdianzi (40.65°N, 117.10°E), which is located about 100 km northeast of suburban Beijing, and the maximum daily average 8-h concentrations of ozone appear to have been >100 ppbv in March 2015 based on Fig. 2 in their paper. High $PM_{2.5}$ and submicron aerosol concentrations have been observed in Beijing (Zhang et al., 2013; Sun et al., 2015). Ozone and aerosol concentrations may therefore have been high in March 2015 over Northeast Asia.

Based on these lidar data and the in-situ measurement data at Takagimachi in Saga city, an air mass with high ozone and aerosol concentrations could have been transported from the free troposphere to the surface by vertical mixing when the planetary boundary layer developed in the daytime. A similar high-surface-ozone event was observed by eight ozonesonde measurements during 6–9 June 2003 over the Seoul metropolitan region (Oh et al., 2010). The combination of ozone DIAL measurements with surface in-situ ozone measurements is very useful for studying the process of descent of high ozone concentrations in the free troposphere to the surface and the impacts on surface air quality. Such measurements of pollution plumes that descend from the free troposphere to the surface are highly recommended (HTAP, 2010).

The MRI-CCM2 could approximately reproduce the high-ozone volume-mixing ratios after some modifications of physical and chemical parameters. MASINGAR mk-2 successfully predicted high aerosol concentration events, but the predicted peak AOD was about one-third of the observed AOD. For further improvement of these models, it will be important to continue comparing these models with ozone DIAL, Mie lidar, and surface in-situ ozone and particle measurements.

Acknowledgements. We used radiosonde data measured by the Japan Meteorological Agency and hourly concentrations of surface oxidant and $PM_{2.5}$ measured by the Saga Prefectural Environmental Research Center. The NOAA Hybrid Single Particle Lagrangian Integrated Trajectory (HYSPRIT) model was used to calculate backward trajectories of air parcels.

Atmos. Chem. Phys. Discuss., doi:10.5194/acp-2016-520, 2016
Manuscript under review for journal Atmos. Chem. Phys.
Published: 22 June 2016

Atmospheric Chemistry and Physics Discussions

265

References

270

Bak, J., Kim, J. H., Liu, X., Chance, K., and Kim, J.: Evaluation of ozone profile and tropospheric ozone retrievals from GEMS and OMI spectra, Atmos. Meas. Tech., 6, 239-249, doi:10.5194/amt-6-239-2013, 2013.

Carslaw, D. C.: Evidence of an increasing NO_2/NO_x emissions ratio from road traffic emissions, Atmos. Env., 39, 4793-4802, 2005.

275 Cattrall, C., Reagan, J., Thome, K., and Dubovik, O.: Variability of aerosol and spectral lidar and backscatter and extinction ratios of key aerosol types derived from selected Aerosol Robotic Network locations, J. Geophys. Res., 110, D10S11, doi:10.1029/2004JD005124, 2005.

Deushi, M. and Shibata, K.: Development of a Meteorological Research Institute Chemistry-Climate Model version 2 for the study of tropospheric and stratospheric chemistry, Pap. Meteorol. Geophys., 62, 1-46, doi:10.2467/mripapers.62.1, 2011.

280 Draxler, R. R. and Hess, G. D.: An overview of the HYSPLIT_4 modeling system for trajectories, dispersion, and deposition, Aust. Meteor. Mag., 47, 295-308, 1998.

Fernald, F. G.: Analysis of atmospheric lidar observations: some comments, Appl. Opt., 23, 652-653, 1984.

Granier, C., Bessagnet, B., Bond, T., D'Angiola, A., van der Gon, H. D.., Frost, G. J., Heil, A., Kaiser, J. W., Kinne, S., Klimont, Z., Kloster, S., Lamarque, J. -F., Liousse, C., Masui, T., Meleux, F., Mieville, A., Ohara, T., Raut, J.-C., Riahi,

285 K., Schultz, M. G., Smith, S. J., Thompson, A., van Aardenne, J., van der Werf, G. R., and van Vuuren, D. P.: Evolution of anthropogenic and biomass burning emission of air pollutants at global and regional scales during the 1980–2010 period, Clim. Change, 109, 163–190, 2011.

Hemispheric Transport of Air Pollution (HTAP) 2010, Part A: Ozone and particulate matter, edited by: Dentener, F., Keating, T., and Akimoto, H., Air Pollution Studies No. 17, United Nations, New York and Geneva, 278 pp., 2010.

290 Houweling, S., Hartmann, W., Aben, I., Schrijver, H., Skidmore, J., Roelofs, G.-J., and Breon, F.-M.: Evidence of systematic errors in SCIAMACHY-observed CO_2 due to aerosols, Atmos. Chem. Phys., 5, 3003-3013, 2005.

Intergovernmental Panel on Climate Change (IPCC): Climate Change 2013: The Physical Science Basis: Contribution of Working Group I to the Fifth Assessment Report of the Intergovernmental Panel on Climate Change, edited by: Stocker, T.F., Qin, D., Plattner, G.-K., Tignor, M., Allen, S.K., Boschung, J., Nauels, A., Xia, Y., Bex, V., and Midgley, P.M.,

295 Cambridge University Press, Cambridge, United Kingdom and New York, NY, USA, 1535 pp,

doi:10.1017/CBO9781107415324, 2013.

Kobayashi, E., Uchiyama, A., Yamazaki, A., and Matsuse, K: Application of the maximum likelihood method to the inversion algorithm for analyzing aerosol optical properties from sun and sky radiance measurements, J. Meteor. Soc. Jpn., 84, 1047-1062, 2006.

Krotkov, N. A., McLinden, C. A., Li, C., Lamsal, L. N., Celarier, E. A., Marchenko, S. V., Swartz, W. H., Bucsela, E. J., Joiner, J., Duncan, B. N., Boersma, K. F., Veefkind, J. P., Levelt, P. F., Fioletov, V. E., Dickerson, R. R., He, H., Lu, Z., and Streets, D. G.: Aura OMI observations of regional SO_2 and NO_2 pollution changes from 2005 to 2015, Atmos. Chem. Phys., 16, 4605-4629, doi:10.5194/acp-16-4605-2016, 2016.

Kurokawa, J., Ohara, T., Morikawa, T., Hanayama, S., Janssens-Maenhout, G., Fukui, T., Kawashima, K., and Akimoto, H.: Emissions of air pollutants and greenhouse gases over Asian regions during 2000–2008: Regional Emission inventory in ASia (REAS) version 2, Atmos. Chem. Phys., 13, 11019–11058, doi: 10.5194/acp-13-11019-2013, 2013.

Ma, Z., Xu, J., Quan, W., Zhang, Z., Lin, W., and Xu, X.: Significant increase of surface ozone at a rual site, north of eastern China, Atmos. Chem. Phys., 16, 3969-3977, doi:10.5194/acp-16-3969-2016, 2016.

Oh, I.-B., Kim, Y.-K., Hwang, M.-K., Kim, C.-H., Kim, S., and Song, S.-K.: Elevated ozone layers over the Seoul metropolitan region in Korea: evidence for long-range ozone transport from eastern China and its contribution to surface concentrations, J. Appl. Meteor. and Climat., 49, 203-220, doi:10.1175/2009JAMC2213.1, 2010.

Ohara, T., Akimoto, H., Kurokawa, J., Horii, N., Yamaji, K., Yan, X., and Hayasaka, T.: An Asian emission inventory of anthropogenic emission sources for the period 1980-2020, Atmos. Chem. Phys., 7, 4419-4444, doi:10.5194/acp-7-4419-2007, 2007.

Ohyama, H., Kawakami, S., Shiomi, K., and Miyagawa, K.: Retrievals of total and tropospheric ozone from GOSAT thermal infrared spectral radiances, IEEE Trans. Geosci. Remote Sens., 50, 1770-1784, doi:10.1109/TGRS.2001.2170178, 2012.

Sakai, T., Nagai, T., Nakazato, M., Mano, Y., and Matsumura, T.: Ice clouds and Asian dust studied with lidar measurements of particle extinction-to-backscatter ratio, particle depolarization, and water-vapor mixing ratio over Tsukuba, Appl. Opt., 42, 7103-7116, 2003.

Stein, A. F., Draxler, R. R., Rolph, G. D., Stunder, B. J. B., Cohen, M. D., and Ngan, F.: NOAA's HYSPLIT atmospheric transport and dispersion modeling system, Bull. Amer. Meteor. Soc., 96, 2059-2077, 2015.

Sun, Y. L., Wang, Z. F., Du, W., Zhang, Q., Wang, Q. Q., Fu, P. Q., Pan, X. L., Li, J., Jayne, J., and Worsnop, D. R.: Long-term real-time measurements of aerosol particle composition in Beijing, China: seasonal variations, meteorological effects, and source analysis, Atmos. Chem. Phys., 15, 10149-10165, doi:10.5194/acp-15-10149-2015, 2015.

Tanaka, T. Y., Orito, K., T. T. Sekiyama, Shibata, K., Chiba, M., and Tanaka, H.: MASINGAR, a global tropospheric aerosol chemical transport model coupled with MRI/JMA98 GCM: Model description, Pap. Meteor. Geophys., 53(4), 119-138, 2003.

Uchino, O., Kikuchi, N., Sakai, T., Morino, I., Yoshida Y., Nagai, T., Shimizu, A., Shibata, T., Yamazaki, A., Uchiyama, A.,

Kikuchi, N., Oshchepkov, S., Brill, A., and Yokota, T., Influence of aerosols and thin cirrus clouds on the GOSAT-observed CO_2: a case study over Tsukuba, Atmos. Chem. Phys., 12, 3393–3404, doi:10.5194/acp-12-3393-2012, 2012a.

Uchino, O., Sakai, T., Nagai, T., Nakamae, K., Morino, I., Arai, K., Okumura, H., Takubo, S., Kawasaki, T., Mano, Y., Matsunaga, T., and Yokota, T., On recent (2008–2012) stratospheric aerosols observed by lidar over Japan, Atmos. Chem. Phys., 12, 11975–11984, doi:10.5194/acp-12-11975-2012, 2012b.

Uchino, O., Sakai, T., Nagai, T., Morino, I., Maki, T., Deushi, M., Shibata, K., Kajino, M., Kawasaki, T., Akaho, T., Takubo, S., Okumura, H., Arai, K., Nakazato, M., Matsunaga, T., Yokota, T., Kawakami, S., Kita, K., and Sasano, Y.: DIAL measurement of lower tropospheric ozone over Saga (33.24°N, 130.29°E) , Japan, and comparison with a chemistry–climate model, Atmos. Meas. Tech., 7, 1385-1394, doi:10.5194/amt-7-1385-2014, 2014.

Veefkind, J. P., Aben, I., McMullan, K., Förster, H., de Vries, J., Otter, G., Claas, J., Eskes, H. J., de Haan, J. F., Kleipool, Q., van Weele, M., Hasekamp, O., Hoogeveen, R., Landgraf, J., Snel, R., Tol, P., Ingmann, P., Voors, R., Kruizinga, B., Vink, R., Visser, H., and Levelt, P. F.: TROPOMI on the ESA Sentinel-5 Precursor: A GMES mission for global observations of the atmospheric composition for climate, air quality and ozone layer applications, Remote Sens. Environ., 120, 70-83, 2012.

Wang, Y., Konopka, P., Liu, Y., Che, H., Müller, R., Plöger, F., Riese, M., Cai, Z., and Lü, D.: Tropospheric ozone trend over Beijing from 2002-2010: ozonesonde measurements and modeling analysis, Atmos. Chem. Phys., 12, 8389-8399, doi:10.5194/acp-12-8389-2012, 2012.

Yue, X. and Unger, N., Ozone vegetation damage effects on gross primary productivity in the United States, Atmos. Chem. Phys., 14, 9137-9153, doi:10.5194/acp-14-9137-2014, 2014.

Yukimoto, S., Adachi, Y., Hosaka, M., Sakami, T., Yoshimura, H., Hirabara, M., Tanaka, T. Y., Shindo, E., Tsujino, H., Deushi, M., Mizuta, R., Yabu, S., Obata, A., Nakano, H., Koshiro, T., Ose, T., and Kitoh, A.: A new global climate model of the Meteorological Research Institute: MRI-CGCM3 —Model Description and Basic Performance—, J. Meterol. Soc. Jpn., 90A, 23-64, doi:10.2151/jmsj.2012-A02. 2012.

Zhang, R., Jing, J., Tao, J., Hsu, S.-C., Wang, G., Cao, J., Lee, C. S. L., Zhu, L., Chen, Z., Zhao, Y., and Shen, Z.: Chemical characterization and source apportionment of $PM_{2.5}$ in Beijing: seasonal perspective, Atmos. Chem. Phys., 13, 7053-7074, doi:10.5194/acp-13-7053-2013, 2013.

Atmos. Chem. Phys. Discuss., doi:10.5194/acp-2016-520, 2016
Manuscript under review for journal Atmos. Chem. Phys.
Published: 22 June 2016

Atmospheric Chemistry and Physics Discussions

Table 1. Characteristics of Mie lidar

Transmitter			
Laser	Nd:YAG		
Wavelength	532 nm	1064 nm	
Pulse energy	130 mJ	130 mJ	
Pulse repetition rate	10 Hz		
Pulse width	8 ns		
Beam divergence	0.2 mrad	0.2 mrad	
Receiver			
Telescope type	Schmidt Cassegrain		
Telescope diameter	30.5 cm		
Focal length	3048 mm		
Field of view	1 mrad		
Polarization	P and S	None	
Number of channels	3	1	
Interference filter			
Center wavelength	532.0 nm	1064.1 nm	
Bandwidth (FWHM)	0.29 nm	0.38 nm	
Transmission	0.66	0 .58	
Detectors	PMT (Hamamatsu R3234-01)	APD (EG&G C30956EH)	
Signal processing	12bit A/D + Photon counting		
Time resolution	1 min		
Vertical resolution	7.5 m		

Atmos. Chem. Phys. Discuss., doi:10.5194/acp-2016-520, 2016
Manuscript under review for journal Atmos. Chem. Phys.
Published: 22 June 2016

Atmospheric Chemistry and Physics Discussions

Table 2. Characteristics of tropospheric ozone DIAL system

Transmitter					
Pump laser	Nd:YAG				
Wavelength	266 nm				
Pulse energy	107 mJ				
Pulse repetition rate	10 Hz				
Pulse width	8 ns				
Raman active gas	CO_2				
Stokes lines	276 nm	287 nm	299 nm	312 nm	
Pulse energy	7.5 mJ	9.1 mJ	8.4 mJ	No. meas.	
Beam divergence	0.1 mrad				
Receiver					
Telescope type	Newtonian			Prime focus (fiber coupled)	
Telescope diameter	49 cm			10 cm	
Focal length	1750 mm			320 mm	
Field of view	1 mrad			3 mrad	
Interference filter					
Center wavelength	287.2 nm	299.0 nm	312.0 nm	276.1 nm	287.2 nm
Bandwidth (FWHM)	1.02 nm	1.15 nm	0.82 nm	1.07 nm	1.05 nm
Transmission	0.18	0.32	0.36	0.17	0.21
Detectors	PMT (Hamamatsu R3235-01)				
Signal processing	12bit A/D + Photon counting				
Time resolution	1 min				
Vertical resolution	7.5 m				

Atmos. Chem. Phys. Discuss., doi:10.5194/acp-2016-520, 2016
Manuscript under review for journal Atmos. Chem. Phys.
Published: 22 June 2016

435 **Figure 1.** Mie lidar and ozone DIAL (right) were installed in the container at the left on the ground (left).

440

445

450

455

Atmos. Chem. Phys. Discuss., doi:10.5194/acp-2016-520, 2016
Manuscript under review for journal Atmos. Chem. Phys.
Published: 22 June 2016

Atmospheric Chemistry and Physics Discussions

(a)

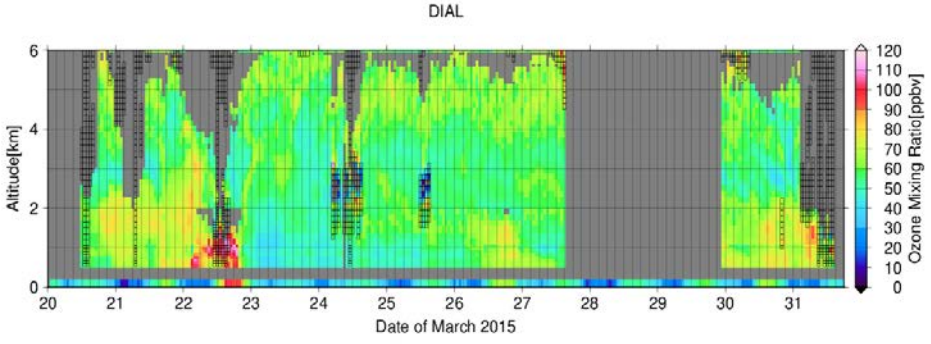

(b)

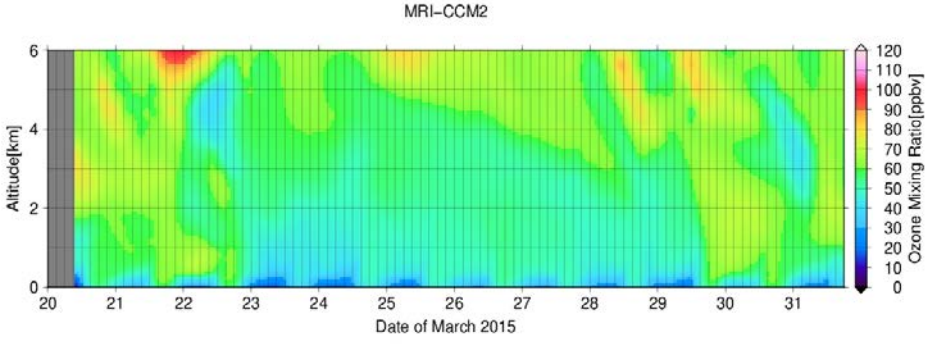

(c)

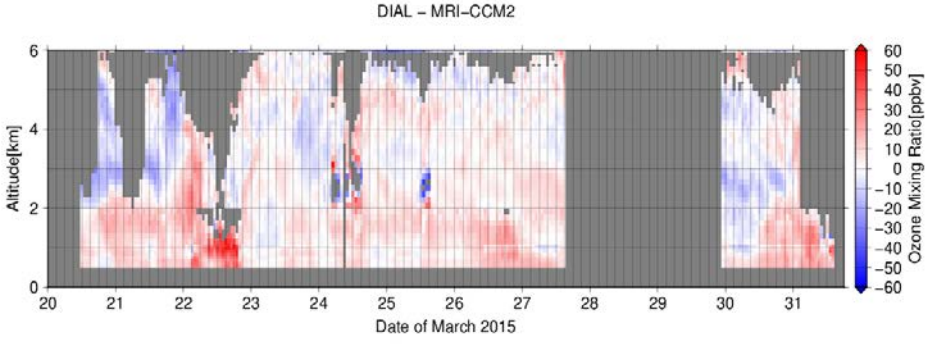

Figure 2. Time-altitude cross-sections of (a) ozone volume mixing ratios observed by DIAL over Saga from 11:10 JST on 20 March to 14:33 JST on 31 March 2015, (b) the ratios simulated by a modified MRI-CCM2 for 20–31 March 2015, and (c) the difference between the observed and simulated ozone volume mixing ratios (a–b). Gray regions indicate areas where there were no observational data or the statistical errors were larger than 10%. Regions enclosed with black rectangles are areas where the data were affected by aerosols and/or clouds. The lowest row in Fig. 2a shows photochemical oxidant (ozone) volume mixing ratios at Takagimachi in Saga city as measured by the Saga Prefectural Environmental Research

Atmos. Chem. Phys. Discuss., doi:10.5194/acp-2016-520, 2016
Manuscript under review for journal Atmos. Chem. Phys.
Published: 22 June 2016

Atmospheric Chemistry and Physics Discussions

Center.

(a)

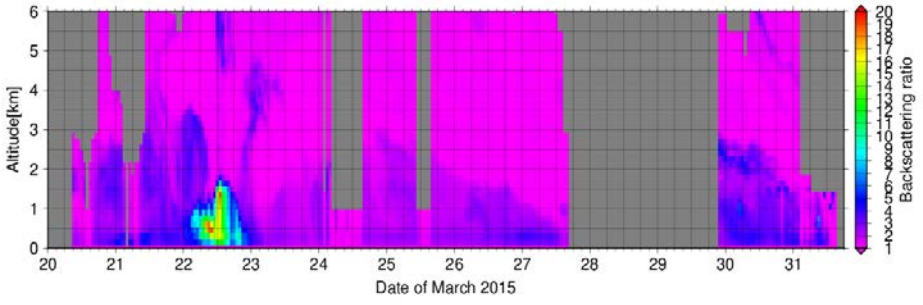

(b)

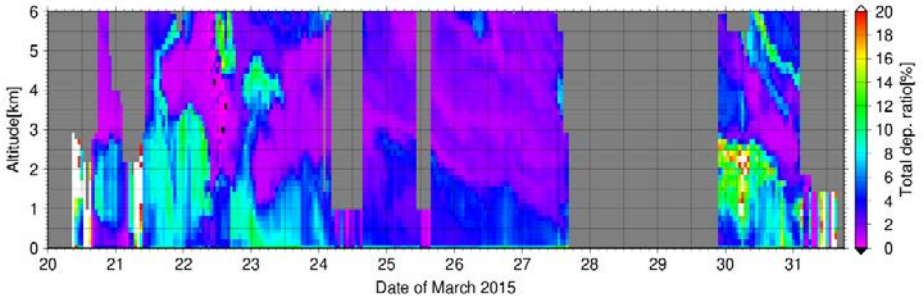

475

Figure 3. Time-altitude cross-sections of (a) backscattering ratios and (b) total volume depolarization ratios at 532 nm observed by Mie lidar at Saga from 11:10 JST on 20 March to 14:33 JST on 31 March 2015. Lidar observations were not available from 15:56 JST on 27 March to 21:58 JST on 29 March 2015 mainly because of bad weather. Gray regions are areas where there were no observational data or where the observations were affected by clouds.

480

485

Atmos. Chem. Phys. Discuss., doi:10.5194/acp-2016-520, 2016
Manuscript under review for journal Atmos. Chem. Phys.
Published: 22 June 2016

Atmospheric Chemistry and Physics Discussions

490

(a)

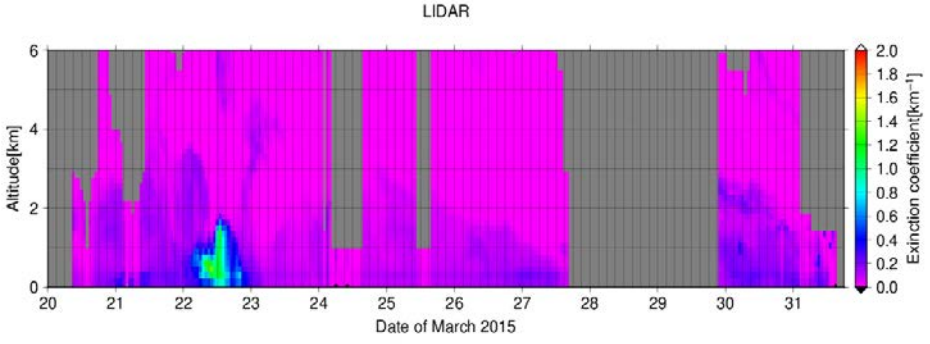

(b)

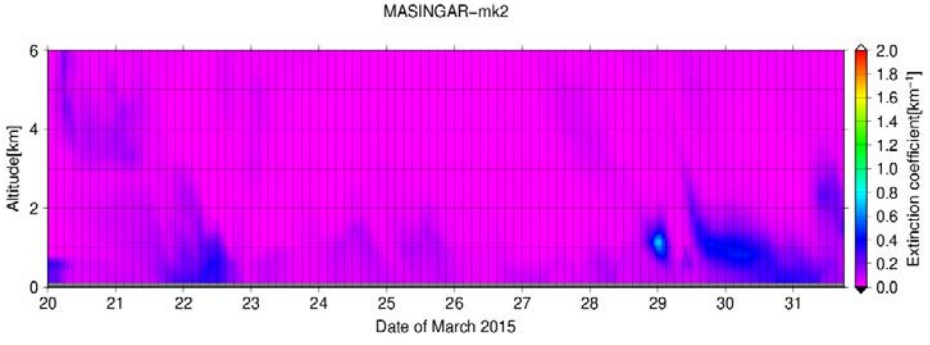

495 (c)

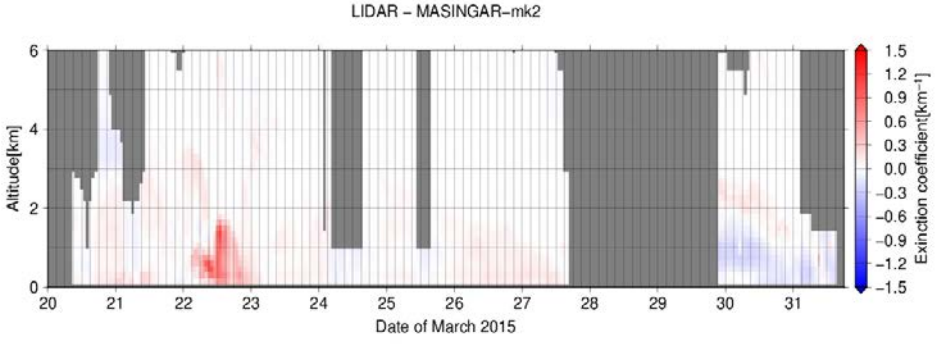

Figure 4. Time-altitude cross-sections of (a) aerosol extinction coefficients observed by Mie lidar at 532 nm over Saga from 11:10 JST on 20 March to 14:33 JST on 31 March 2015, (b) the coefficients simulated by MASINGAR-mk2 at 550 nm for
500 20–31 March 2015, and (c) the difference between the Mie lidar observations and the simulation (a–b). Gray regions represent areas where there were no observational data.

Atmos. Chem. Phys. Discuss., doi:10.5194/acp-2016-520, 2016
Manuscript under review for journal Atmos. Chem. Phys.
Published: 22 June 2016

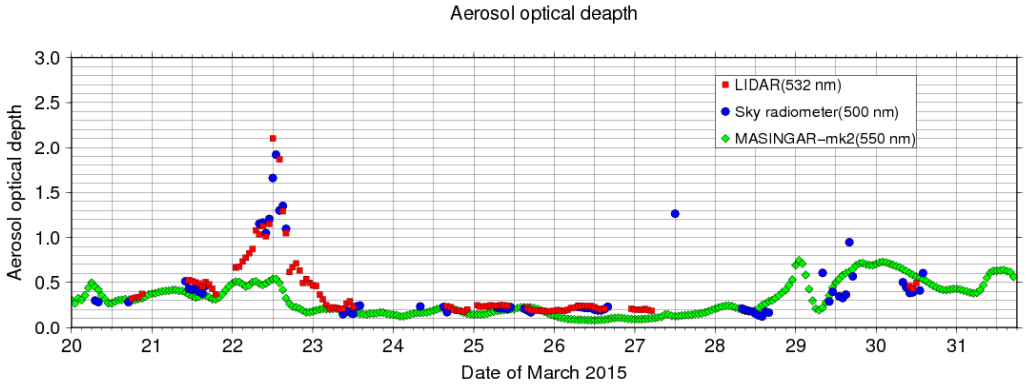

Figure 5. Temporal variation of the aerosol optical depth (AOD) measured by Mie lidar at 532 nm (red circles), by sky radiometer at 500 nm (blues circles), and simulated at 550 nm by MASINGAR-mk2 (green circles).

Atmos. Chem. Phys. Discuss., doi:10.5194/acp-2016-520, 2016
Manuscript under review for journal Atmos. Chem. Phys.
Published: 22 June 2016

Atmospheric Chemistry and Physics Discussions

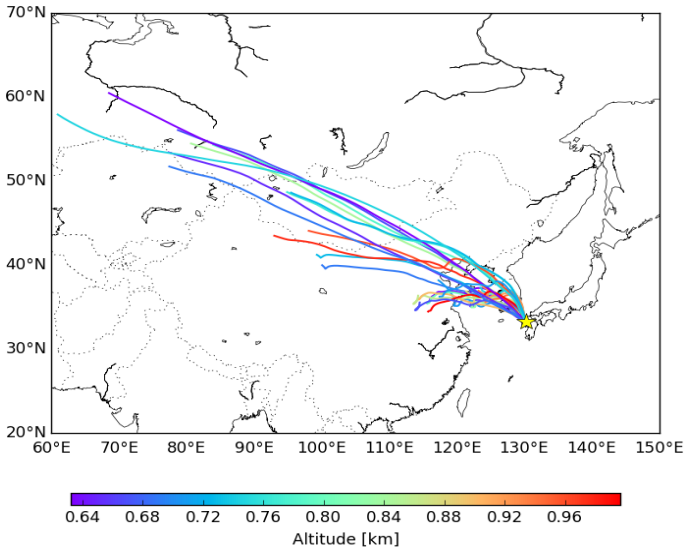

Figure 6. Horizontal projections of three-dimensional backward trajectories of 27 air parcels initially at altitudes of 600–1000 m over the lidar site at Saga. The colors show the initial positions of the air parcels. The trajectories were calculated for three days from 00:00 UTC (09:00 JST) on 22 March 2015 by the NOAA HYSPLIT trajectory ensemble option using the 1° × 1° Global Data Assimilation System (http://ready.arl.noaa.gov/hypub-bin/trajtype.pl?runtype=archive).